



Contents lists available at ScienceDirect

# Journal of Rock Mechanics and Geotechnical Engineering

journal homepage: [www.jrmge.cn](http://www.jrmge.cn)

## Full Length Article

# Temperature dependence of mechanical properties and damage evolution of hot dry rocks under rapid cooling

Longjun Dong<sup>a</sup>, Yihan Zhang<sup>a</sup>, Lichang Wang<sup>b,\*</sup>, Lu Wang<sup>b</sup>, Shen Zhang<sup>a</sup><sup>a</sup>School of Resources and Safety Engineering, Central South University, Changsha, 410083, China<sup>b</sup>School of Geosciences and Info-physics, Central South University, Changsha, 410083, China

## ARTICLE INFO

### Article history:

Received 22 December 2022

Received in revised form

3 August 2023

Accepted 14 August 2023

Available online 20 November 2023

### Keywords:

Hot dry rock

Acoustic emission

Mechanical properties

High temperature

Damage

## ABSTRACT

Understanding the differences in mechanical properties and damage characteristics of granitoid under high temperatures is crucial for exploring deep geothermal resources. This study analyzes the evolution of the acoustic emission (AE) characteristics and mechanical parameters of granodiorite and granite after heating and water cooling by uniaxial compression and variable-angle shear tests under different temperature gradients. We identify their changes in mesostructure and mineral composition with electron probe microanalysis and scanning electron microscopy. Results show that these two hot dry rocks have similar diagenetic minerals and microstructure, but show significantly different mechanical and acoustic characteristics, and even opposing evolution trends in a certain temperature range. At the temperatures ranging from 100 °C to 500 °C, the compressive and shear mechanical properties of granodiorite switch repeatedly between weakening and strengthening, and those of granite show a continuous weakening trend. At 600 °C, both rocks exhibit a deterioration of mechanical properties. The damage mode of granite is characterized by initiating at low stress, exponential evolutionary activity, and intensified energy release. In contrast, granodiorite exhibits the characteristics of initiating at high stress, volatile evolutionary activity, and intermittent energy release, due to its more stable microstructure and fewer thermal defects compared to granite. As the temperature increases, the initiation and propagation of secondary cracks in granodiorite are suppressed to a certain extent, and the seismicity and brittleness are enhanced. The subtle differences in grain size, microscopic heterogeneity, and mineral composition of the two hot dry rocks determine the different acoustic-mechanical characteristics under heating and cooling, and the evolution trends with temperature. These findings are of great significance for the scientific and efficient construction of rock mass engineering by rationally utilizing different rock strata properties.

© 2024 Institute of Rock and Soil Mechanics, Chinese Academy of Sciences. Production and hosting by Elsevier B.V. This is an open access article under the CC BY-NC-ND license (<http://creativecommons.org/licenses/by-nc-nd/4.0/>).

## 1. Introduction

Geothermal resources, characterized as renewable and environmentally friendly energy sources, have gained prominence as a vital resource supply (Bai et al., 2012; Wei et al., 2015; Zhao et al., 2015a, 2017a). Hot dry rock formations serve as the predominant reservoir for these resources. Under high temperature and cooling conditions, the mineral composition, internal structure, and mechanical properties of hot dry rocks are profoundly changed (Ohno, 1995; Zhang and Sun, 2018; Wu et al., 2019). Understanding the

mechanical behavior and failure mechanism of hot dry rock in the thermal environments is crucial for geothermal resource exploration and utilization.

At present, some consensus have been reached on the temperature dependence of the compressive (Kumari et al., 2017; Yang et al., 2019), shear (Zhang et al., 2018a; Ma et al., 2020) and tensile (Zhao et al., 2018; Guo et al., 2020) strength characteristics of hot dry rocks under varying stress conditions. Thermal damage to these rocks under different temperature gradients mainly includes real-time high-temperature damage (Zhao et al., 2017b; Ma et al., 2020; Li et al., 2021) and cooling damage (Kumari et al., 2017; Wu et al., 2019). The latter usually refers to the damage caused by liquid nitrogen LN2 rapid cooling, water cooling, and natural cooling (Ma et al., 2021; Xiao et al., 2022). Granitoids are the most widely distributed hot dry rocks and their physical and mechanical

\* Corresponding author.

E-mail address: [wlccsu@csu.edu.cn](mailto:wlccsu@csu.edu.cn) (L. Wang).

Peer review under responsibility of Institute of Rock and Soil Mechanics, Chinese Academy of Sciences.

properties usually experience a transition from strengthening to weakening at high temperatures, appearing different temperature thresholds (Liu and Xu, 2014; Yang et al., 2019; Wu et al., 2021). Macroscopically, the brittle failure mode changes to the plastic failure mode, showing more obvious ductility. Microscopically, the microstructure further weakens at higher temperatures (Talukdar et al., 2018), increasing the number and width of internal transgranular cracks (Huang et al., 2017; Ma et al., 2021). At high temperatures, rock grains undergo anisotropic thermal expansion and mineral composition transformation (Ohno, 1995; Chen et al., 2017); after being rapidly cooled, the scales of cleavage and fracture are enlarged. The higher the cooling rate (LN2 cooling > water cooling > natural cooling), the more severe the damage to the rock microstructure, resulting in a significant degradation of the rock physical and mechanical properties (Kumari et al., 2017; Zhang et al., 2018a; Wu et al., 2019; Yin et al., 2022). In addition, increasing heating and cooling cycles intensifies the damage to the rock structure. Granite shows strong ductility and obvious post-peak behavior (Ge and Sun, 2018). Moreover, the thermal effects on physical and mechanical changes of the granite with different grain sizes were more significant at high temperature (Kang et al., 2021). Some studies (Chen et al., 2014; Su et al., 2017) have focused on the relationship between rockburst tendency and temperature under different stress environments. Within a relatively low-temperature range, higher temperatures may increase rock brittleness, and induce more intense rockburst.

The acoustic emission (AE) phenomenon is caused by transient elastic energy release during rock micro-fracture process (Dong et al., 2023a). AE signals not only reflect the characteristics of fracture sources (Kong et al., 2021; Kwiatek et al., 2014; Dong et al., 2019), but also capture rock structural information (Brantut, 2018; Dong et al., 2021a; 2023b). Moreover, AE signals exhibit high sensitivity to various internal and external conditions during rock failure (Dong et al., 2021b; Liu et al., 2020a). AE characteristic parameters and waveforms not only characterize the spatio-temporal evolution process of the initiation, propagation and coalescence of rock cracks (Xu and Zhang, 2018; Dong et al., 2020, 2022a), but also provide key information for understanding the scale-frequency relationship and fracture mechanism of microcracks (AE sources) (Xing et al., 2019; Dong et al., 2022b). Many studies tended to reveal the crack propagation law of the rocks that have different degrees of thermal damage, using the variation of energy, counts, and hits/events in AE characteristic parameters (Liu et al., 2020b; Yang et al., 2022). They found that the accumulated number and growth rate of AE count in granite significantly reduced after the relatively high-temperature treatment (Yang et al., 2019). The slope of the AE energy evolution curve of sandstone at the late deformation stage increases first and then decreases from 25 °C to 1000 °C, reflecting the transition from brittleness to ductility (Xiao et al., 2022). The reduction of the shear-type microcracks proportion indicates that increasing temperature has a negative effect on the effectiveness of hydraulic fracturing (Xing et al., 2019). In addition, the  $b$  value was introduced to measure the relative relationship between the micro-crack scale and frequency in rock failure under the effect of temperature. Increasing heating and cooling cycles leads to a larger  $b$  value but suppresses the AE activity during rock instability (Ge and Sun, 2018). Chmel and Shcherbakov (2014) found that as temperature increased, the statistical form of the  $b$  value of granite with different particle sizes under impact load gradually transformed from Gutenberg–Richter type to Poisson type. Stress-strain or AE methods can effectively determine the characteristic stress points of rock crack propagation (Zhao et al., 2015b). The relative temporal changes at the rock failure stages are used to evaluate the thermal damage and crack development process of the hot dry rock. The rock crack initiation threshold stress and the crack damage

threshold stress increase with growing temperature, including Beishan granite (Xiao et al., 2022) and Australian Strathbogie granite (Kumari et al., 2017). There is also a turning point in the variation trend of the characteristic stress point in a certain temperature range (Chen et al., 2018). However, for macroscopically similar granitoid, the mechanical and acoustic evolution trends may present completely different temperature dependencies within a specific temperature range. Understanding the seismicity and mechanical characteristics of different reservoir rocks is essential to the strategies for geothermal resource drilling and the safe construction of rock mass engineering. Additionally, limited studies have explored the impact of a single microscopic factor on the macroscopic mechanical properties of rocks, and the control of rock damage evolution under high temperature and water cooling. A systematic analysis is necessary for comprehending the thermal damage mechanism of reservoir rocks by microscopic attribute.

In this study, we investigated the two variations in compressive and shear mechanical properties of heated reservoir rocks after rapid water cooling from 100 °C to 600 °C. Meanwhile, we conducted a comparative analysis of the temperature-influenced characteristics of damage evolution by combining AE time-series, characteristic stresses, and amplitude frequency distribution. Furthermore, we systematically analyzed different thermal evolution mechanisms influenced by microstructural and mineralogical controlling effects, using electron probe microanalysis (EPMA) and scanning electron microscopy (SEM). This study provides a valuable theoretical reference for geothermal resource exploration and utilization.

## 2. Experimental methodology

### 2.1. Rock description

The rocks in this study are fresh unweathered granite sampled from Dingziwan, Changsha, Hunan Province, China and granodiorite from Longhai District, Zhangzhou, Fujian, China (Fig. 1a and b). Dingziwan is located at Wangcheng-Zhuzhou fault zone (Fxiang-00030), which has a length of 115 km, with a fault plane striking 320° and dipping 50°. It is believed that a hidden secondary NW-trending fault extends to a depth of 25 km. Along the two sides of this fault zone, many hot springs are mainly distributed. The southeast coast of China, represented by Zhangzhou, Fujian Province, boasts abundant geothermal resources. The maximum temperature of the drilled geothermal water reaches 121.5 °C, located at a depth of 100 m beneath downtown Zhangzhou. The two rock specimens were thinly sliced for mineral composition analysis (Fig. 1c–f). The granite specimens are greyish-white, massive structure, and medium-to-coarse-grained, with a few dark-colored mafic minerals, most of which are biotite and partially altered to chlorite. The grain size of granite minerals ranges from 0.5 mm to 2.5 mm. The average density of granite is 2.6 g/cm<sup>3</sup> at natural temperature. The main minerals are alkaline feldspar, accounting for 41% of the composition. The secondary minerals are medium acid plagioclase (26%), quartz (27%), muscovite (5%), and biotite (1%). The accessory mineral is fluorite. The granodiorite ranges between 0.5 mm and 2 mm in mineral particle size and the average density of granodiorite is 2.76 g/cm<sup>3</sup> at natural temperature. The mineral specimen is grey-green, darker than that of granite, as it has more dark-colored mafic minerals and fewer quartz particles. It is considered a neutral igneous rock, with neutral plagioclase being the main mineral component at 70%. The secondary minerals include biotite (12%), alkaline feldspar (8%), amphibole (6%), pyroxene (2%), and quartz (2%).

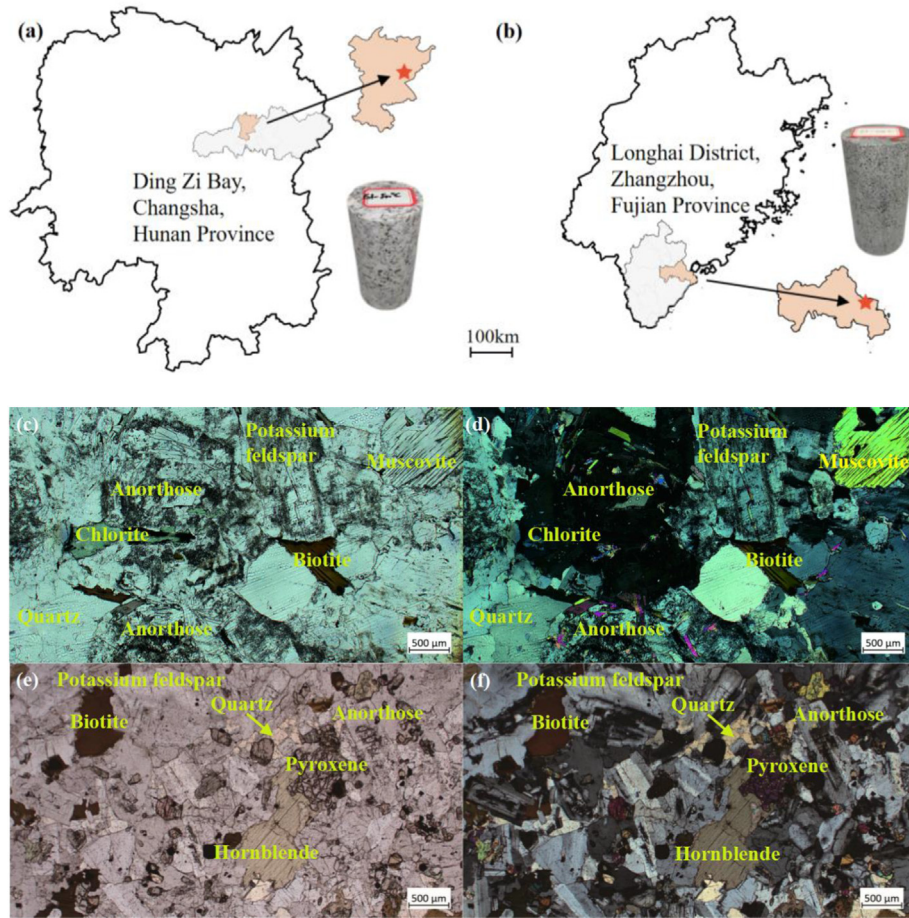


**Fig. 1.** The sampling location, specimen and EPMA photos of the specimens under natural state: (a) Granite, (b) Granodiorite, (c) Orthogonal polarization spectral image of granite, (d) Single polarization spectral image of granite, (e) Orthogonal polarization spectral image of granodiorite, and (f) Single polarization spectral image of granodiorite.

## 2.2. Specimen preparation

The granite and granodiorite were cut and polished into cylindrical tubes, following International Society for Rock Mechanics (ISRM) standards for flatness and verticality. The dimensions of the specimens are 50 mm in diameter and 50 mm, 30 mm, and 100 mm in height (Hudson and Ulusay, 2007). The specimens with 50 mm and 30 mm in height were used for 50° and 60° variable-angle shear tests, respectively, and the specimens with 100 mm in height were used for uniaxial compression tests. All specimens were dried in an oven at 50 °C for 24 h. Then, they were heated in a muffle furnace. The set heating rate was 5 °C/min, and the target temperatures were 100 °C, 200 °C, 300 °C, 400 °C, 500 °C, and 600 °C. After heating at the target temperature for 3 h, the specimens were taken out and put into iron buckets filled with water at 20 °C. The water was continuously injected for circulation to rapidly cool the specimens. Finally, the cooled specimens were left to dry naturally in a ventilated place. The specimen type and heating temperature of each specimen were marked.

## 2.3. Microscopic examination

The rock specimens treated at 200 °C, 400 °C, and 600 °C were cut into small cubes with a side length of 5 mm and coated with gold sputtering by an E-1010 ion sputter to enhance conductivity. Then, the microstructure of the rock surface under different temperature gradients was observed with the JSM-IT200 digital

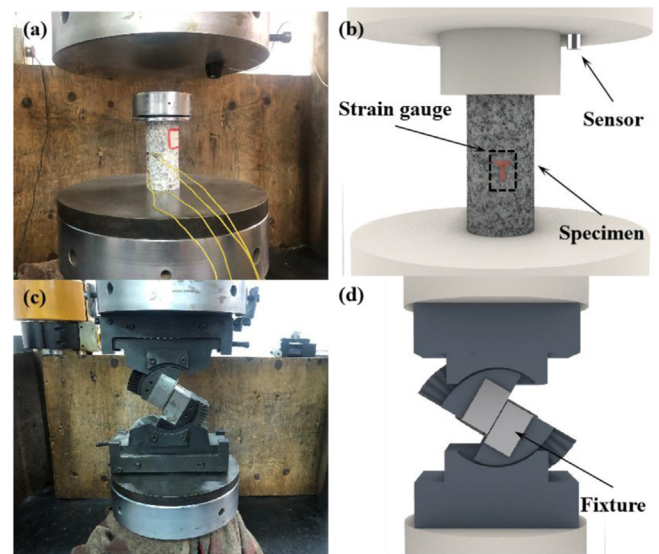


**Fig. 2.** Experimental system: (a) A photo of the uniaxial compression test, (b) The model of the uniaxial compression test, (c) A photo of the variable-angle shear experiment, and (d) The model of variable-angle shear experiment.

scanning electron microscope. The observation size ranges from 10 μm to 50 μm. The results were recorded by photographing.



## 2.4. Mechanical test and AE monitoring

The INSTRON 1346 electro-hydraulic servo universal testing machine was used to perform both uniaxial compression tests and variable-angle shear tests ( $50^\circ$  and  $60^\circ$ ) on granite and granodiorite (Fig. 2). Displacement control was used in the uniaxial compression test, and the loading rate was set to 0.1 mm/min. In the center of the side of each specimen, a pair of 5 mm strain gages are placed in a "T" sub-shape along the axial and vertical axes. They were used to measure the transverse strain and axial strain. Two channels of the DH5921 dynamic strain gauge are respectively connected with transverse and axial strain gages to collect data. The AE acquisition system and sensor were PCI-2 and GTMicro300, respectively. The sensor was magnetically attached to the pressure head of the testing machine. In AE monitoring, the sampling frequency was set to 10 MHz and the threshold value was set to 45 dB.

The experimental framework for the entire study is presented in Fig. 3.

## 3. Experimental results

### 3.1. Effect of temperature on the microstructure

We compared the photographs of the granite mineral thin slices after heating at 200 °C, 400 °C, and 600 °C and water-cooling (Fig. 4) with those at the normal temperature (Fig. 2a and b). At 25 °C–200 °C, there is minimal change in the granite minerals, and a few cracks appear on the slices after the temperature reaches 200 °C. With increasing temperature, feldspar alteration is pronounced, resulting in uneven protrusions. Additionally, the blackening of biotite and pyroxene occurred due to the precipitation of iron and magnesium minerals, leading to increased opacity. Moreover, higher temperature results in larger and more crystal fissures in the mineral flakes. During water cooling, high-temperature minerals rapidly condense and shrink, leading to further development of mineral cleavage. Once the temperature reaches 600 °C, a large number of intercrystalline cracks and transgranular cracks appear in the minerals, which are interlaced.

The EPMA results of granodiorite are shown in Fig. 5. When the temperature reaches 600 °C or above, the mineral structure of

granodiorite exhibits a fragmented pattern. Some minerals reach a critical melting point and form many interlaced microcracks and small cracks. As the temperature continues to increase, crystal cracks in the rock become more pronounced, leading to the development of mineral cleavage. The granite and granodiorite slices show similar temperature-induced changes, differing mainly in their mineral composition and structure.

### 3.2. Fracture morphology analysis

Understanding the microstructure changes of hot dry rocks after heating and water cooling is the key to revealing the physical and mechanical properties as well as the crack evolution. In Fig. 6, the microstructure changes of granite and granodiorite are observed at an interval of 200 °C. After the granite is heated at 200 °C and water-cooled, the gaps, pores, and microcracks appear (Fig. 6a). Minerals are densely distributed, and mineral particles are obvious. Microcracks are irregularly distributed along the gaps and pores, showing signs of initiation but not yet expansion or penetration. The minerals are tightly connected in the form of flakes, and heat flow and rapid water cooling have obvious impacts on these flakes. As shown in Fig. 6b, granodiorite has a similar distribution of gaps and pores, the development of microcracks, and the arrangement compared to granite. However, the density of small mineral flakes in granodiorite is smaller than that of granite at the same temperature.

After being heated at 400 °C and water-cooled, in granite and granodiorite, the gaps almost disappear, and the pores become less noticeable. However, the microcracks extensively form, and gradually evolve into large cracks. Compared with that heated at 200 °C, the density of flake minerals is much lower, and large cracks are linearly connected. The heat flow and rapid cooling impact also have obvious influences on these flakes, causing them to enlarge. The figure reveals a distinct light white section on the right, possibly resulting from intrusive substances during heating and rapid cooling of the crystalline rock. These findings support the idea that high temperature and rapid cooling accelerate pore closure, crack development, mineral fracturing, and large crack penetration. At the same temperature, the mineral flake size of granodiorite is larger and more complete than that of granite (Fig. 6c and d).

After heating at 600 °C and water-cooling, the granite microstructure has no gaps or obvious pores (Fig. 6e), but large cracks form, connect, and gradually expand. Two small cracks expand and connect, splitting the rock into blocks, and generating microcracks that develop continuously. The rock structure is smooth, with a few protruding mineral flakes. Due to the heat flow, the mineral particles disperse, and clear boundaries form between minerals and crystal particles. Large cracks traversing the rocks appear as straight lines or smoother curves. Most sections extend along mineral boundaries, a few sections pass through minerals, and very few sections may cut through crystal particles. Coalescence of microcracks and small cracks is observed, which splits the overall mineral structure at high temperatures and forms mineral fragments and particles. The high temperature of 600 °C and rapid cooling accelerate the formation and penetration of large cracks and rapidly expand the cracks in terms of opening, depth, and length. Finally, the effects of rapid cooling and heat flow have more significant effects on granodiorite (Fig. 6e).

In summary, as the temperature rises, the number, opening, depth and length of cracks in the granite increase, while the original gaps and pores gradually decrease. The microcracks merge and intensify, creating different shaped blocks with smaller fragments. The grain boundaries of mineral bodies become more distinct and scattered as a result of thermal damage and cooling impact. Large cracks appear as straight lines or smooth curves. The higher the

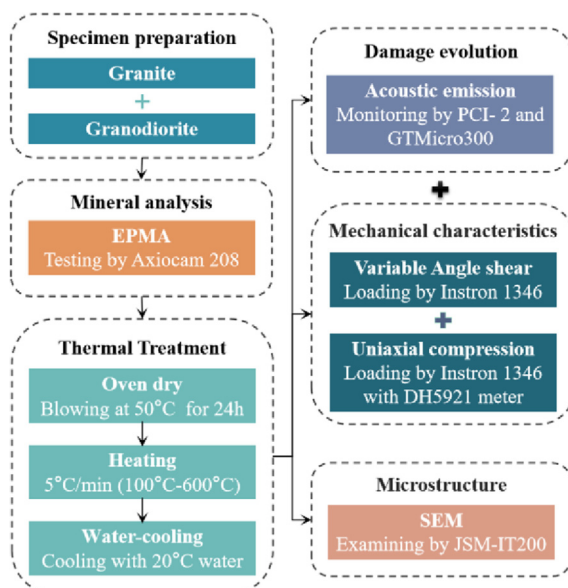
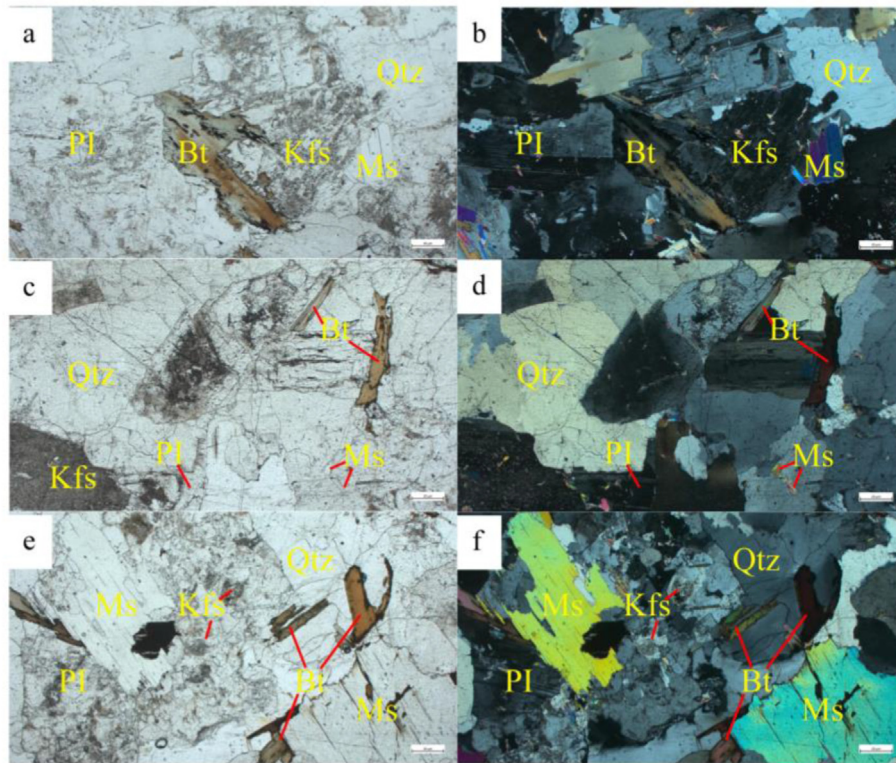
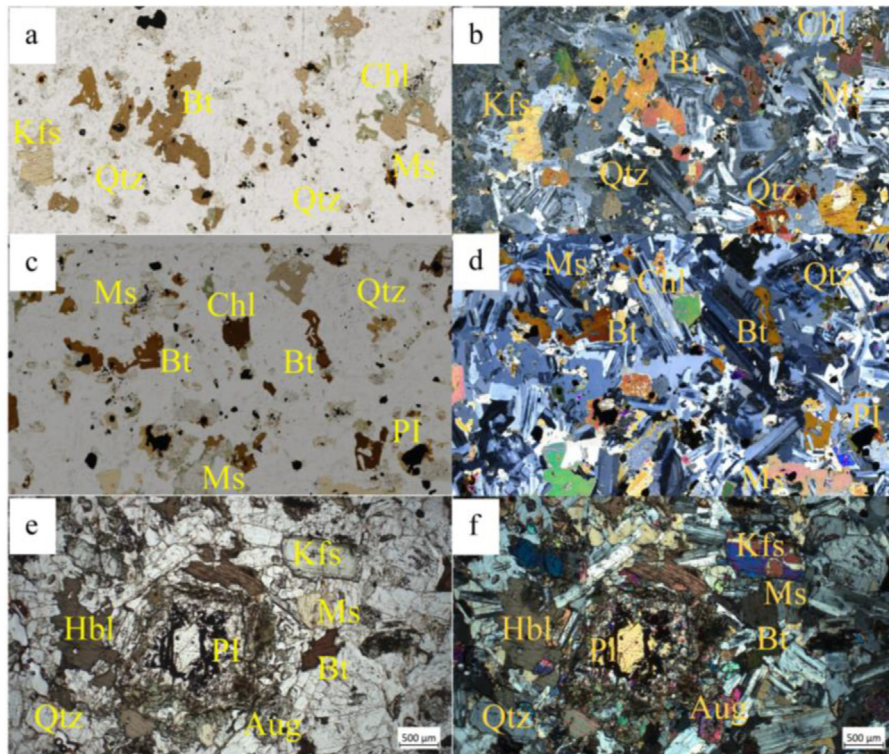


Fig. 3. Flowchart of the experiment.



**Fig. 4.** EPMA photographs of the granite thin slice after heating at (a, b) 200 °C, (c, d) 400 °C and (e, f) 600 °C and water-cooling. The left panel shows the single polarization photographs, and the right panel shows the orthogonal polarization photographs. Qtz – Quartz, Bt – Biotite, Ms – Muscovite, Kfs – K-feldspar, Pl – Fluorite.



**Fig. 5.** EPMA photographs of the granodiorite thin slice after heating at (a, b) 200 °C, (c, d) 400 °C and (e, f) 600 °C and water-cooling. The left panel shows the single polarization photographs, and the right panel shows the orthogonal polarization photographs. Qtz – Quartz, Chl – Chlorite, Pl – Plagioclase, Kfs – K-feldspar, Bt – Biotite, Ms – Muscovite, Hbl – Hornblende, Aug – Augite.



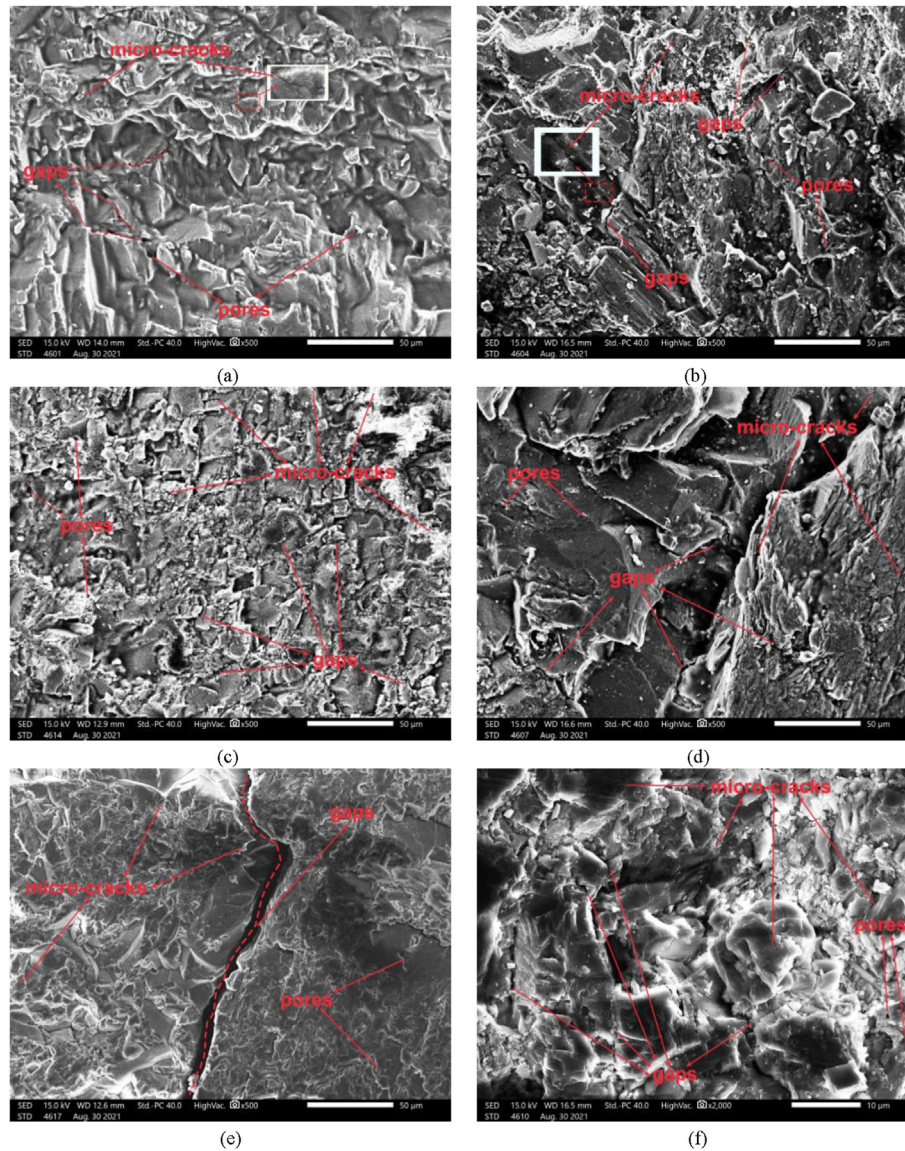


**Fig. 6.** Microstructures of the granite (left panel) and granodiorite (right panel) being heated at (a, b) 200 °C, (c, d) 400 °C, and (e, f) 600 °C.

temperature, the stronger the crack resistance to the weak mineral boundary in the extension, the more obvious the linearity of large cracks. As the temperature increases, thermal fractures become more apparent. The heat flow effect is significant in the fracture converging area, demonstrated by the scattered rock fragments and mineral particles, and clear boundaries of crystal particles. Water cooling enhances the fragmentation and damage of the micro-particles of granodiorite, and accelerates the formation, development, and coalescence of large cracks. However, it can relatively suppress the formation of microcracks, and ensure the integrity of single rock fragments. The fracture development of granodiorite is lower than that of granite.

### 3.3. Stress-strain response

The stress-strain curves of granite and granodiorite specimens under uniaxial compression are shown in Fig. 7. The strength and deformation change significantly with temperature. The stress-strain curves of both granite and granodiorite experienced a process of "linearly elastic" to "elasto-plastic" and then to "plasto-elasto-plastic", but their transition temperature thresholds are

different. In addition, the granite has more obvious negative lateral displacement under moderate temperature and low loading. These changes reflect that after high-temperature heating and water cooling, the accumulation of thermal damage and development of microcracks increase, leading to a gradual transition from brittle failure to brittle plastic failure. As the temperature increases, the mechanical properties of granite gradually deteriorate. The stress-strain curves exhibit increasingly apparent compaction and plastic stage, along with increased plasticity and lateral deformation. In contrast, granodiorite undergoes a transition between strengthening and weakening of mechanical properties at the temperatures of 200 °C–400 °C. The linearly elastic characteristics remain unchanged up to 500 °C, as shown by the stress-strain curves. However, at 600 °C, granodiorite shows plastic behavior that is different from the strain characteristics of brittle rock.

### 3.4. Compression characteristics

Fig. 8 illustrates the variation characteristics of mechanical indices with temperature under uniaxial compression and the results of the linear fitting. The shaded part along the fitting lines

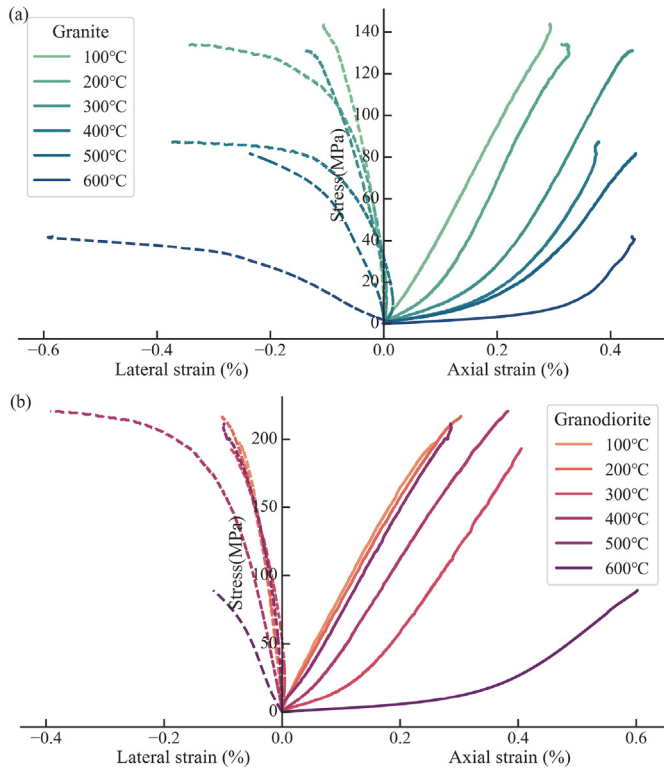


Fig. 7. Stress-strain curves of (a) granite and (b) granodiorite.

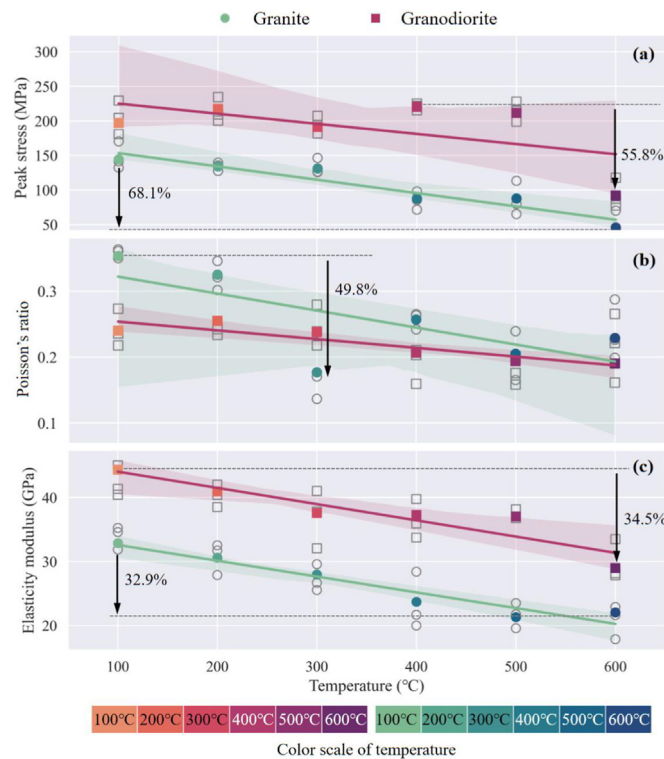


Fig. 8. (a) Peak stress, (b) Poisson's ratio, and (c) elasticity modulus of the two rocks at different temperatures.

corresponds to the 95% confidence interval of the fitting results. The index values of the two rocks all decrease with rising temperature.

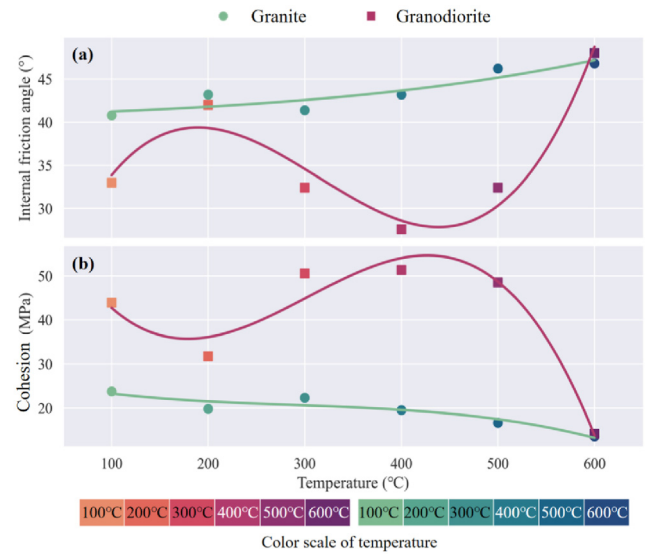


Fig. 9. (a) Friction angle and (b) cohesion of the two rocks at different temperatures.

However, granodiorite exhibits greater rigidity, as its peak strength and elastic modulus are larger than those of granite, and the Poisson's ratio is smaller under the same high temperatures.

At the low temperatures, the uniaxial compressive strength of granodiorite has no great changes. It fluctuates within 30 MPa around 200 MPa from 100 °C to 500 °C, and reaches the peak at 400 °C. When the temperature reaches 600 °C, the peak strength plunges by 55.8%. On the other hand, the uniaxial compressive strength of granite continues to reduce with rising temperature, and two most apparent reductions occur at 300 °C and 600 °C, which reduces by 33.3% and 44.7%, respectively. From 100 °C to 600 °C, the uniaxial compressive strength reduces by 68.1%, which is more significant than granodiorite. The elastic moduli of the two hot dry rocks show a gradual decline trend with the increasing temperature. When the temperature reaches 600 °C, the elastic moduli of granite and granodiorite decrease by 32.9% and 34.5%, respectively. The Poisson's ratio shows a decreasing trend with the increasing temperature. At 300 °C, the Poisson's ratio of granite drops by 49.8% and rises to a certain extent after reaching 400 °C. In some studies, the Poisson's ratio decreases first and then increases at 300 °C (Kumari et al., 2017) and 370 °C (Wu et al., 2019). However, such change is not obvious in this study. To sum up, granodiorite has higher strength, stiffness, and brittleness and can maintain stable mechanical properties at lower temperatures. Granite shows higher ductility after heating and water cooling. These differences are related to the microstructure changes. The reduction of the loading ability is due to the microscopic damage. The variations of structural damage and mineral properties of the rock caused by heating and water cooling also change the rock physical properties. The transition from brittle to plastic is directly reflected by the changes in elastic modulus and Poisson's ratio.

### 3.5. Shear characteristics

We did the variable-angle shear tests and calculated the cohesion ( $c$ ) and internal friction angle ( $\varphi$ ) of granite and granodiorite after heating and water cooling to further analyze the temperature effects on the shear strength. Fig. 9 shows the variations of  $c$  and  $\varphi$  as well as the results of the cubic polynomial fitting. The  $c$  of the two rocks shows an increasing-decreasing trend, as the temperature increases, while the  $\varphi$  shows a decreasing-increasing trend.



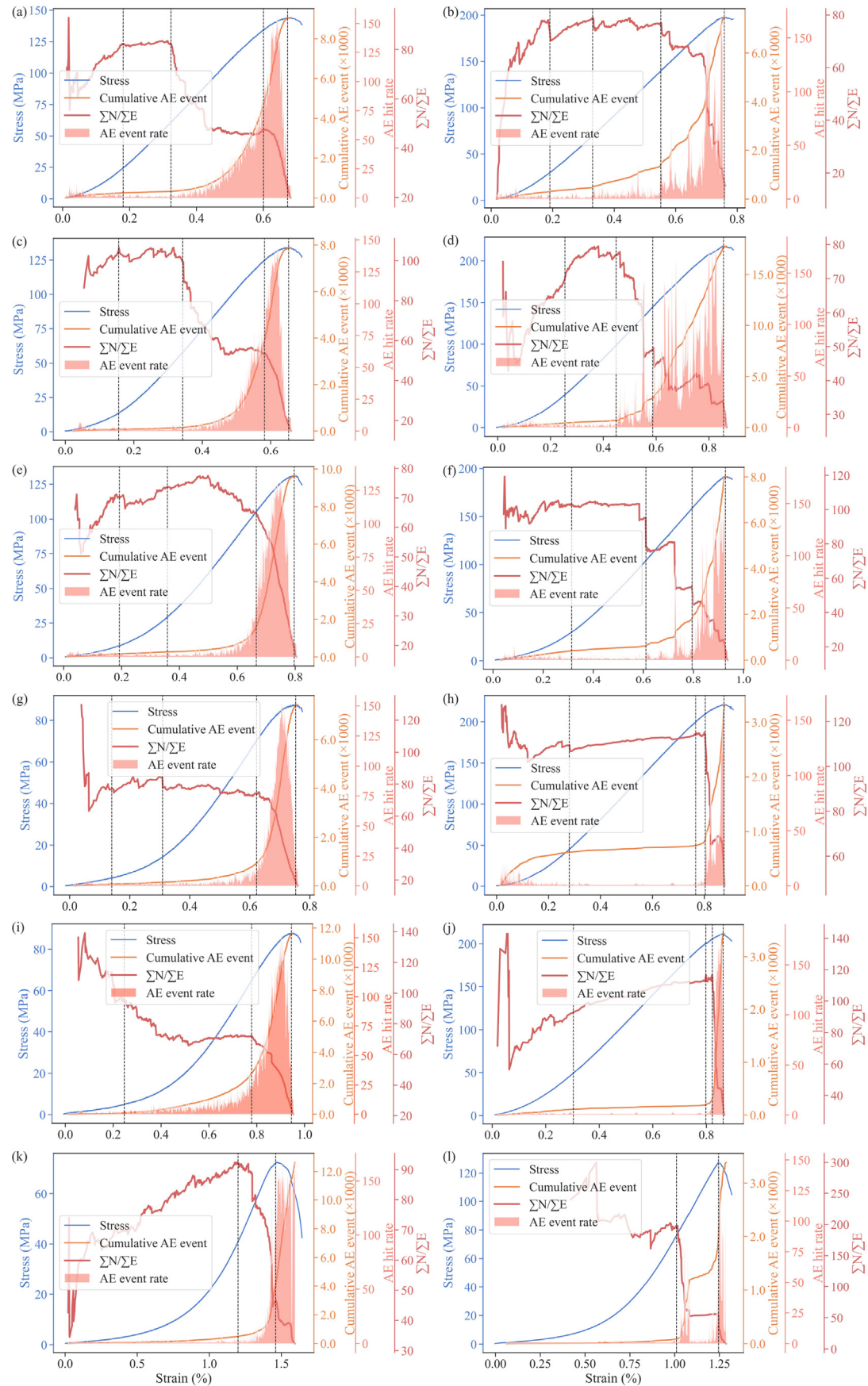


**Fig. 10.** Stress and AE evolution curves of granite (left panel) and granodiorite (right panel) at (a, b) 100 °C, (c, d) 200 °C, (e, f) 300 °C, (g, h) 400 °C, (i, j) 500 °C, and (k, l) 600 °C.



These trends are coincident with the results of many studies (Zhang et al., 2018b; Ma et al., 2020). Under the same temperature gradients, the  $c$  of granite is generally smaller but the  $\phi$  is larger than those of granodiorite. The shear resistance of granite reduces with a temperature threshold of 300 °C. The  $c$  and  $\phi$  of granodiorite experience substantial decreases, converging to values similar to those of granite at 600 °C. The trends in shear strength and compressive strength for both rocks have certain similarities, as observed from the critical temperatures of around 500 °C for granodiorite and 300 °C for granite. These temperatures signify noteworthy reductions in their respective shear and compressive strengths.

Differences between laboratory test results and field data often arise due to uncertainties such as rock heterogeneity discreteness, and sampling errors. To ensure reliability in rock engineering design, the mechanical properties must be probabilistically characterized. The frequentist method can effectively calculate the potential distribution of data and analyze the changing trend, as shown in the calculation of confidence interval and polynomial fit in Figs. 8 and 9. Also, Bayesian approaches can be utilized to quantify uncertainty in mechanical properties for subsurface engineering applications (Bao and Burghardt, 2022; Feng et al., 2021). The changes of  $c$  and  $\phi$  are related to the influences of thermal hardening and thermal cracking on the overall internal structure of the rocks. The microstructure changes show that granodiorite can endure thermal shock damage better than granite, as fewer thermal cracks appear. Therefore, it can maintain a stable microstructure within 500 °C and keep the shear properties. Moreover, granite contains plenty of quartz, which has a higher expansion coefficient than other diagenetic minerals. This leads to a more pronounced mineral deformation mismatch and reduced inter-mineral contacts, ultimately weakening the shear resistance properties.

### 3.6. AE hit and energy model evolution characteristics

At present, geothermal resource exploration involves temperatures up to 500 °C. The above analysis shows that the mechanical properties of granite and granodiorite deteriorate significantly at 600 °C, and the values of mechanical indices become similar. However, within 500 °C, granodiorite and granite have significantly different evolutionary trends. To understand these trends in the geothermal exploration environment, this study investigates the damage evolution characteristics by AE at the temperatures ranging from 100 °C to 500 °C. Fig. 10 shows the AE hit and  $\sum N/\sum E$  evolution of the two rocks with loading at different temperatures.  $\sum N/\sum E$  represents the ratio of the cumulative AE hit to the cumulative AE energy, describing the concentration of the AE energy release. According to the phase trend characteristics, the  $\sum N/\sum E$  curve in the whole process is segmented using the dotted line.

The initial stress of AE activity in granite is low. The frequency of AE hits progressively increases as a power function and the overall AE process is relatively active. At 100 °C–500 °C, the number of cumulative AE hits increases from about 8000 to about 12,000. We define the time interval below  $\sum N/\sum E = 95$  as the relatively active period of energy release. The granite active period expands with the rising temperature. After heating and water cooling, the damage of granite is more developed, suggesting that temperature promotes the AE activity during the uniaxial compression. On the other hand, the initial stress of AE activity in granodiorite is relatively high, and the frequency of AE hits is characterized by intermittent increasing and large-scale oscillations. The cumulative AE hits start decreasing continuously from 200 °C to about 3500. Its active period of energy release is shorter, indicating that the temperature significantly suppresses the AE activity of granodiorite in the damage process.

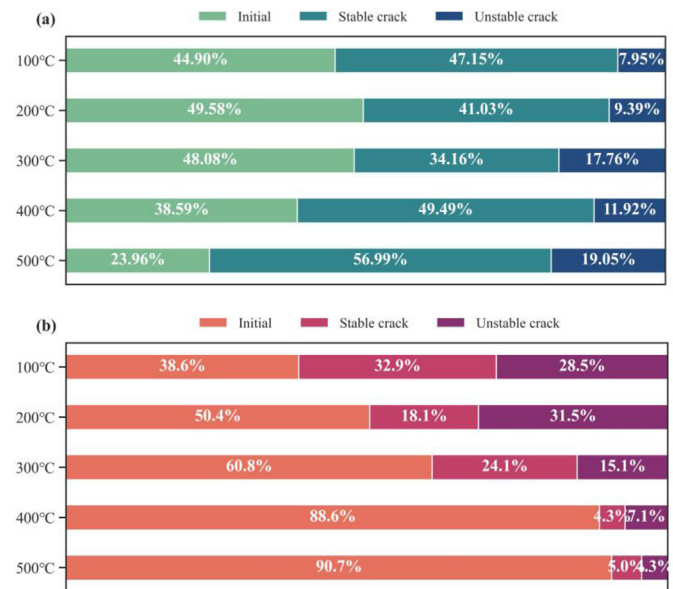
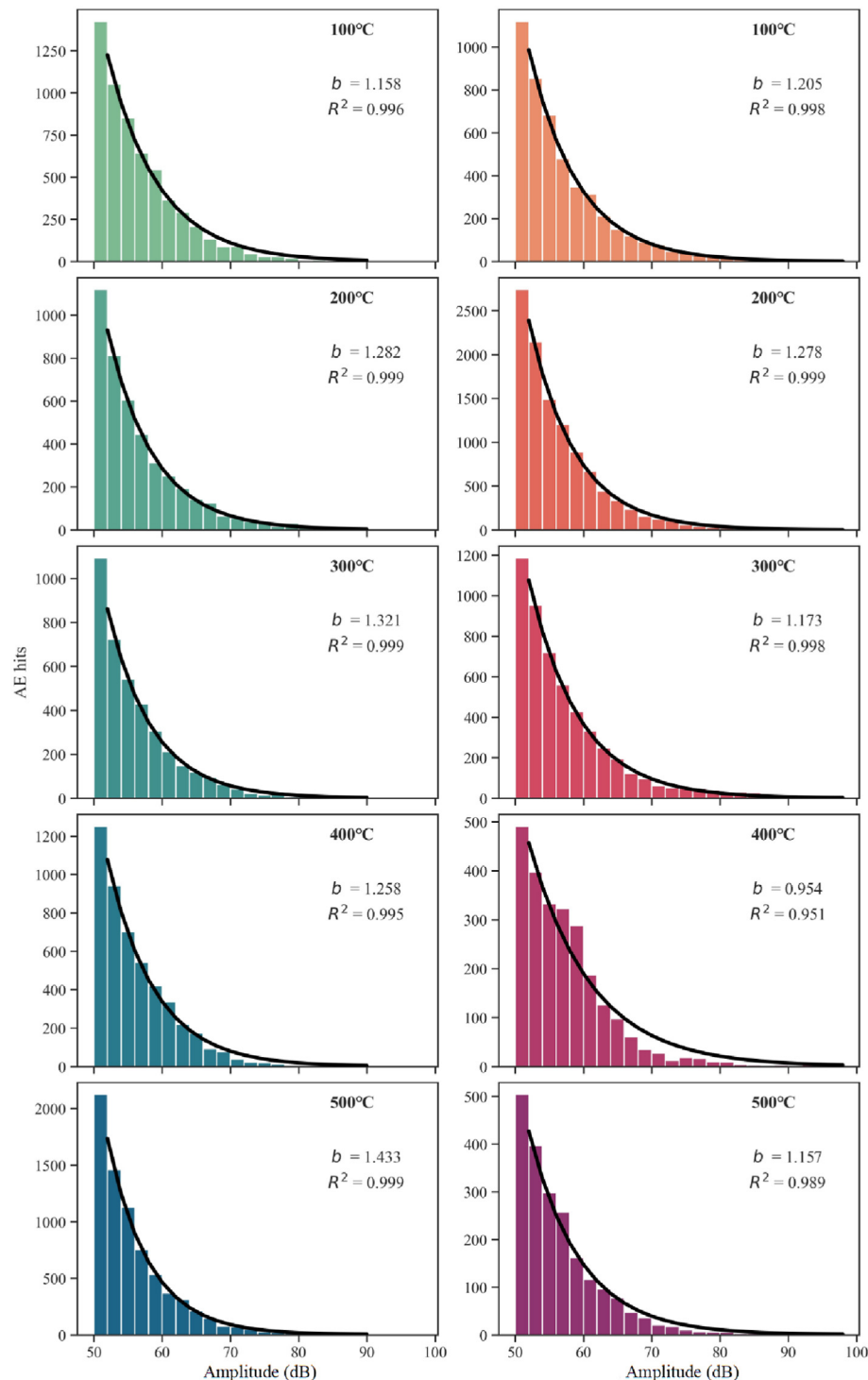


Fig. 11. Comparisons of the proportions of different stages in rock failure at different temperatures: (a) Granite and (b) Granodiorite.

The sudden drop of  $\sum N/\sum E$  indicates that the AE energy release density intensifies rapidly after the rock enters the secondary crack growth stage. The steady fluctuation of  $\sum N/\sum E$  suggests a stable equilibrium in the scale of secondary cracks during the stable crack growth. The AE energy release processes of granite and granodiorite are different. During the initial compaction stage, the rock heterogeneity causes stress adjustment, thus the  $\sum N/\sum E$  curves of the two rocks gradually rise and fluctuate. In granite, the micro-crack extending and penetrating are continuous. During the period from plastic deformation to instability, there are two sudden drops in  $\sum N/\sum E$  followed by a period of steady fluctuation between them. As the temperature increases, the descent gradient of  $\sum N/\sum E$  in the last descending period gradually decreases, revealing a relatively smooth release of elastic energy during subcritical crack growth. The mentioned descent gradient represents the ratio of the  $\sum N/\sum E$  difference to the strain difference within the same interval. Differently, the  $\sum N/\sum E$  variation of granodiorite forms a multi-step decline, reflecting that the multiple secondary primary fractures with time intervals together lead to the rock instability. The damage evolution of granodiorite is not a gradually accelerating process but experiences stress accumulation and adjustment. As the temperature increases, the number of  $\sum N/\sum E$  declining steps decreases, and the energy release concentrates in the later part of time scale.

At 600 °C, the two rocks show significant AE phenomena after the peak stress, with fewer AE events before the peak, deviating from typical brittle rock failure patterns within 500 °C. In the case of more severe thermal damage to the rock at 500 °C, attenuation of AE signals with high frequency is more pronounced during the early loading stage, resulting in missing AE signal acquisition under plastic deformation. These AE signals typically originate from small-scale micro-fractures caused by compression and closure. In addition, premature initiation of secondary microcracks in a low-stress environment leads to the penetration of pre-existing large-scale thermally-induced cracks. This leads to a stress drop from the peak value, but the rock's bearing capacity is not entirely lost, allowing continued crack expansion.



**Fig. 12.** The relationships of amplitude frequency distribution and  $b$  value fitting results at different temperatures. Left panel is for granite, and right panel is for granodiorite.

### 3.7. Damage evolution stage characteristics

Combining the inflection points of the trend of  $\Sigma N/\Sigma E$  and cumulative AE curve (Wang et al., 2018), the damage evolution process is divided into three stages: initial stage, stable cracking, and unstable cracking. At the high temperatures, the secondary cracks in granite and granodiorite have opposite extending regulations during AE evolution. As shown in Figs. 10 and 11, the crack initiation stress threshold ( $\sigma_{ci}$ ) and crack damage stress threshold

( $\sigma_{cd}$ ) of granite gradually advanced, and crack growth and unstable growth stage takes a growing proportion in the whole loading process. However,  $\sigma_{ci}$  and  $\sigma_{cd}$  of granodiorite are gradually postponed in the time scale. The relatively quiet period with almost no AE hits is gradually extended. The proportion of crack growth and unstable growth stage gradually decreases with the rising temperature.

These differences reflect two crack growth modes under temperature effects. In Mode 1, the heating and water cooling reduce



the stress threshold of the secondary crack. The pre-existing microcracks caused by thermal damage continue to expand under low stresses. The accumulated elastic energy is released in advance and the state of secondary crack growth is activated earlier. The energy release and crack propagation are gradual and orderly during the entire damage evolution. In Mode 2, within 500 °C, the mechanical properties of granodiorite remain stable. Heating enhances the bonding between mineral particles, causing a partial closure of micro-fissures under thermal stress. This results in an increased capacity of elastic strain energy storage. The stress threshold of the secondary crack increases and the time of crack growth is delayed on time series. It shows that the energy release and crack extension are significantly suppressed in the damage evolution of granodiorite.

### 3.8. *B-value characteristics*

The magnitude in the Gutenberg-Richter relation is replaced with the normalized AE amplitude, as presented in Eq. (1).

$$\log_{10} N(A/20) = a - bA/20 \quad (1)$$

where  $N(A/20)$  represents the frequency of AE within the magnitude statistical interval,  $A$  is the amplitude of AE hit, and  $a$  is an empirical constant.

In addition, the magnitude interval in the magnitude statistics catalog is stipulated as 2 dB. According to the characteristics of power law distribution, the optimal magnitude of completeness is uniformly set as 50 dB in the calculation. The  $b$  value is fitted by the nonlinear least squares method and solved in the form of an exponential function (Liu et al., 2020a).

The amplitude-frequency distributions of all specimens follow the Gutenberg-Richter relationship, and the coefficient of determination ( $R^2$ ) of the  $b$  value is generally close to 1, except for granodiorite at 400 °C and 500 °C (Fig. 12). In granite, there are almost no AE hits higher than 90 dB, due to the premature release of strain energy. In granodiorite, the pre-existing microcrack density is lower, the stress threshold for crack initiation is higher, and more elastic energy accumulates, thus large-scale cracks with higher amplitudes appear. The  $b$  value of granite is higher than granodiorite at the same temperature, reflecting the different intensities of crack growth in the two rocks. In addition, the damage process in granite is more moderate than that in granodiorite.

As the temperature rises, the relationship between AE amplitude and frequency in the micro-fracture evolution shows different trends for granite and granodiorite. The  $b$  value of granite gradually increases from 1.158 to 1.433. With the advance of  $\sigma_{cd}$ , the cracks initiate and propagate under lower stresses, which gradually decreases the proportion of large-scale micro-fractures. The  $b$  value of granodiorite fluctuates around 1.2. Specifically, it is greater than 1.2 under 200 °C and smaller than 1.2 above 300 °C. The deviation of  $b$  value is affected by the low  $R^2$  at 400 °C. The thermal hardening of the microstructure causes a delay in the crack propagation stage. Under higher stresses, larger-scale fractures are initiated during the secondary propagation of the thermal damage crack and the formation of the main fracture. Hence, the proportion of the small-scale fractures gradually decreases.

## 4. Discussion

### 4.1. Differences in temperature dependence

Considering the results of compressive strength, cohesion, elastic modulus,  $\sigma_{ci}$ , and  $b$  value, the relative damage of granite and granodiorite with temperature is calculated using the isotropic

treatment of each index (Fig. 13). The relative thermal damage degree in the two rocks shows completely different trends. Granodiorite maintains the mechanical properties, elastic strain energy storage capacity, and brittleness during the damage evolution within 100 °C–500 °C and even shows a strengthening trend. Further, the relative relationship between thermal hardening and thermal cracking effect can be more intuitively distinguished through the relative damage variable, which is calculated by peak strength, referring to the peak strength at 100 °C, as shown in Fig. 14. The damage variables of granite show a continuous increase, with consistently dominant thermal cracking effect. On the other hand, the damage variables of granodiorite fluctuate below zero, indicating that the thermal hardening mechanism is dominant up to 500 °C.

After heating and cooling, the mechanical properties and structural integrity of rock undergo deterioration transformation. However, it is necessary to distinguish whether a reservoir rock is in a state of strengthening, maintaining or weakening within the specific temperature range of an engineering environment. The above analysis shows that the two typical hot dry rocks, both are granitoids, are intuitively similar but have different microscopic mechanisms of thermal damage, critical temperatures, and mechanical and damage evolution characteristics. The macro-differences in rocks are a comprehensive reflection of rock-forming minerals, microstructure, and structural characteristics.

The microscopic observations through SEM and EPMA showed that granodiorite and granite differ significantly in two aspects:

- (1) Granodiorite contains more fine mineral particles, with a medium-to-fine-grained and massive structure. Granite contains more medium mineral particles, with a medium-to-coarse-grained and porphyritic structure. It has more primary fissures, pores, and gaps at the junction of granite particles. Additionally, the uniformity of the microscopic particles in granite is slightly worse than that of granodiorite.
- (2) Plagioclase is the main rock-forming mineral in granodiorite, accounting for about 70%. However, the proportion of plagioclase, alkaline feldspar, and quartz together account for 70% of granite. Granodiorite contains negligible amounts of quartz, which accounts for nearly 30% of granite. Biotite comprises only 1% of granite, whereas roughly 12% of granodiorite.

Granite and granodiorite undergo a series of physical and chemical changes during heating and cooling. It is necessary to reveal the factors causing different thermal damage mechanisms from the aspects of mineral composition and microstructure. In terms of mineralogy, the rock-forming minerals of the two rocks are similar. The discussion regarding the control of thermal damage mechanisms focuses on the distinct effects of secondary minerals such as quartz and biotite on granite and granodiorite, respectively, along with variations in plagioclase and K-feldspar content. In terms of microstructure and fabric, the dissimilarities in the formation of thermally-induced cracks, mechanical properties, and damage evolution between the two rocks are explored through a comparison of coarse-grained and medium-to-fine-grained sizes, variations in mesoscopic heterogeneity, and the extent of development of primary gaps, pores, and joint fissures.

### 4.2. Mechanisms of temperature-dependent differences

#### 4.2.1. Different thermal damage mechanisms of mechanical properties

Among the main rock-forming minerals of granite and granodiorite, quartz exhibits the highest hardness and elastic modulus,

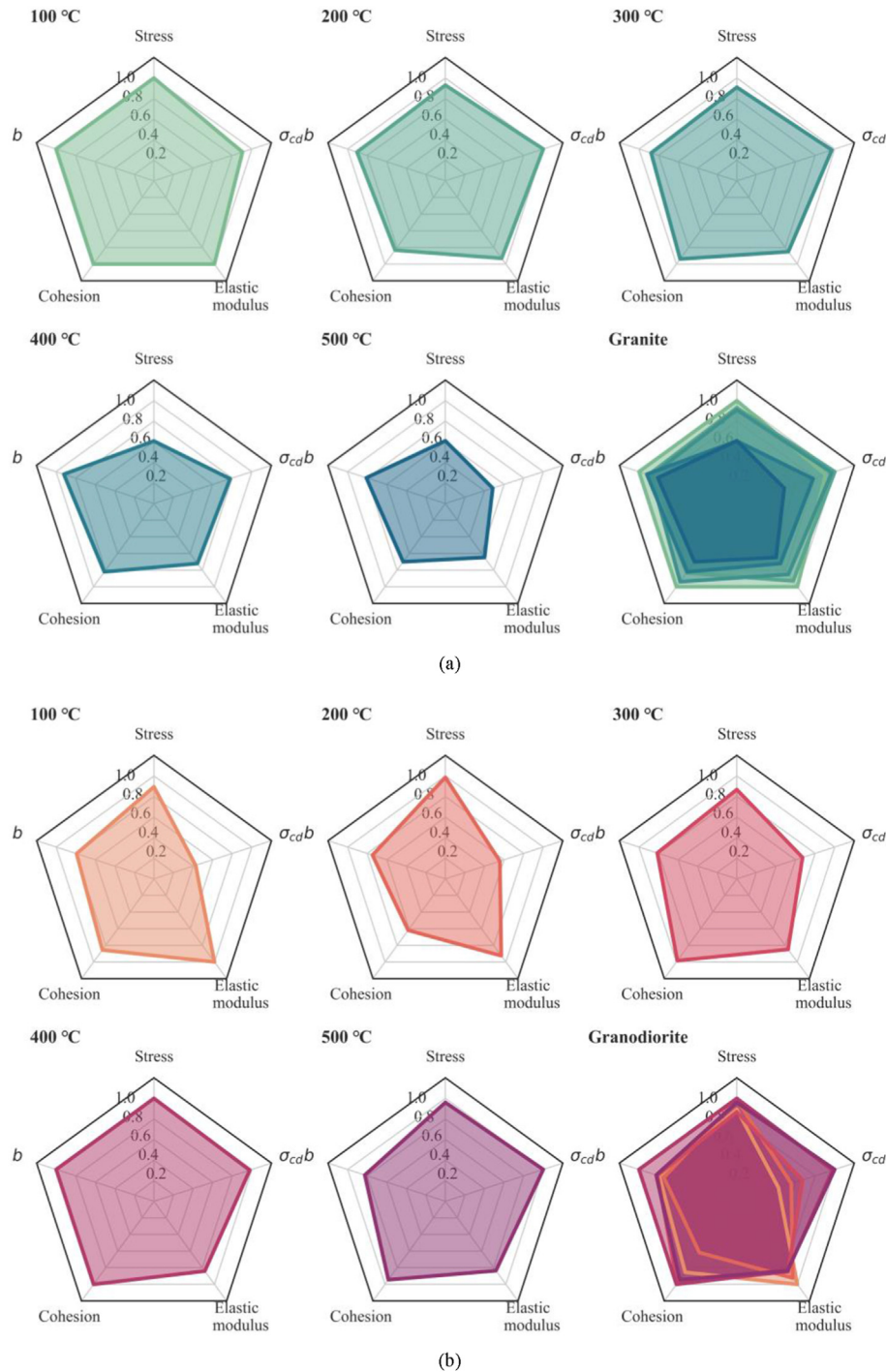


Fig. 13. Comprehensive assessment by relative damage of hot dry rock: (a) Granite and (b) Granodiorite.

and K-feldspar is relatively softer with a slightly lower elastic modulus than plagioclase and amphibole (Prodaivoda et al., 2004). Biotite, as the weakest rock component, has the lowest hardness due to its fragile cleavage planes but exhibits greater toughness when heated. These characteristics determine its essential role in stress distribution, crack formation, and propagation (Mahabadi et al., 2012). Granodiorite has the dominating component of plagioclase, with a minor presence of biotite, pyroxene, amphibole, and quartz. Rock specimens containing large amounts of amphibole and plagioclase phenocrysts exhibit higher uniaxial compressive

strength and initiation stress, while the presence of biotite is inversely proportional to the strength (Ündül et al., 2015). However, the negative effect of a minor biotite content is negligible for granodiorite. In contrast, rock-forming minerals in granite contain a higher proportion of K-feldspar and quartz with larger grain sizes. The low uniaxial compressive strength generally is related to the large alkaline feldspar content and grain size, while the proportion of quartz has no significant statistical correlation with mechanical properties (Güneş Yılmaz et al., 2011; Ündül et al., 2015). Moreover, rock heterogeneity is influenced by pre-existing joint fissures, grain



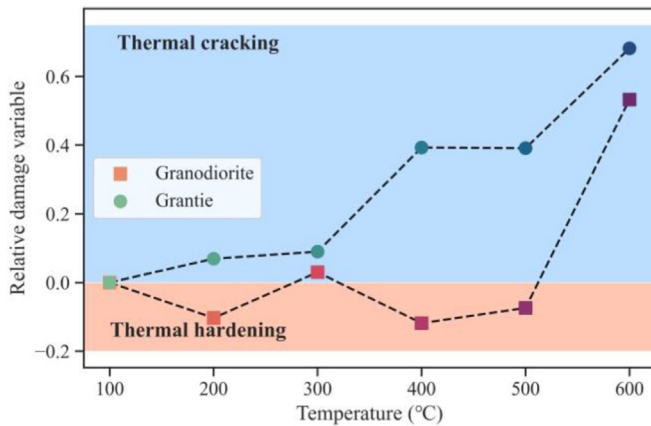


Fig. 14. Comparison of thermal hardening and thermal cracking effect.

boundaries, and local strength attributed to diagenetic minerals. Microscopic observation shows that granite has a larger grain size, and worse uniformity of meso-particles compared to granodiorite. The primary cracks at the grain junction of granites are more developed than those of granodiorite, indicating a higher degree of heterogeneity. This is another factor that determines the differences in macroscopic strength. Microcracks, gaps, and pores basically have no tensile capacity and reduce the cohesion between mineral particles. As the grain size increases, the grain boundary area decreases while the number of pre-existing microcracks, gaps, and pores increases. Consequently, this will lead to a reduction in the stress threshold for friction and dislocation movement between rock particles (Zhao et al., 2018; Peng et al., 2021). Therefore, granite has lower tensile strength and cohesion than granodiorite.

The varying micro-mechanical properties of different minerals at varying temperatures account for the different thermal evolution of strength between the two rocks. Some studies (Zhang et al., 2018b; Li et al., 2020; Mo et al., 2022) have reported a significant decrease in the hardness and elastic modulus of quartz as the temperature increases. Plagioclase and K-feldspar also have a gradually decreasing trend in micro-mechanical properties, and the overall decline is slight. In addition, there is a discernible upward trend observed at temperatures below 300 °C. The mechanical properties of these minerals will be restored to different degrees during cooling. Interestingly, the elastic modulus of plagioclase could be even stronger than that before the heating and cooling treatment. In contrast, the mechanical properties of biotite increase significantly with increasing temperature due to the interlayer spacing contraction along cleavage planes. Among these minerals, quartz experiences the most deterioration in micro-mechanical properties. Plagioclase and alkali feldspar exhibit some improvements in mechanical properties at low-temperature intervals, and the mechanical properties of biotite increase continuously with temperature. The mentioned findings offer support for the preservation of macroscopic mechanical properties in granodiorite within 500 °C, whereas granite's properties continue to deteriorate. On the other hand, as the temperature increases, the thermal cracking effect of granite intensifies. This leads to a significant increase of internal crack density, a decrease of the connection between mineral particles, and a continuous deterioration of the mechanical properties (Chen et al., 2017).

Granodiorite is primarily influenced by thermal hardening at the temperatures below 500 °C. This leads to partial closure of primary microcracks due to thermal expansion, and intensified cohesion between the minerals, resulting in stable mechanical properties within a specific temperature range. The variation in

mineral microscopic properties and thermal shock damage significantly contributes to the difference in the temperature threshold of the transition from brittle to plastic within 600 °C between the two types of rocks. Moreover, plagioclase undergoes a crystalline phase transition at approximately 300 °C (Yang et al., 2016; He et al., 2018), while quartz transforms from  $\alpha$  phase to  $\beta$  phase around 573 °C (Kimizuka et al., 2003; Ohno et al., 2006). These mineral phase transitions cause significant alterations in micro-mechanical properties, which is a fundamental reason for sudden changes in mechanical behavior.

#### 4.2.2. Different thermal damage mechanisms of micro-fracture evolution

The more significant difference in elastic modulus between mineral particles, the more likely it is to generate uncoordinated deformation during thermal expansion and compression loading, forming intergranular cracks. In contrast to granodiorite, which has plagioclase as its sole main rock-forming mineral, granite has the main minerals as quartz, plagioclase, and K-feldspar with similar proportions. The different elastic moduli of the three minerals make it easier to concentrate the stress at the boundary of mineral particles. Additionally, as the grain size increases, the stress concentration at the grain boundaries becomes more pronounced (Lindqvist et al., 2007). Biotite has the lowest elastic modulus, which determines that the initiation and propagation of micro-cracks tend to occur at the phase boundary between it and other minerals in granodiorite. Li et al. (2003) suggested that even a small amount of biotite, as low as 10%, can contribute significantly to the propagation of micro-fractures. In addition to considering differences in mineral composition and lithology, the main factors affecting the AE activity during rock failure are the density and scale of pre-existing cracks (Lei et al., 2000), which are related to the macroscopic inhomogeneity, the development of microscopic joint, and the size of mineral particles. Pre-existing cracks in the specimen cause local stress concentration under loading, which is an important reason for the rock instability and failure. Rocks with larger pre-existing cracks and well-developed joints are more likely to have clustered AE activities, i.e. AE hit rate has large fluctuations temporally and clustered spatially (Lei, 2003, 2017). Larger grain sizes can promote the interaction between cracks (Moura et al., 2005, 2006). During the damage evolution, granite has a higher propensity to generate extensive microcrack activity compared to granodiorite. This is evident by the increased number of accumulated AE events and more fragmented rock fragments after failure.

Further, we summarized two modes of rock damage evolution and crack propagation in granite and granodiorite. The mechanism of crack evolution in granite is controlled by pre-existing defects, large grain sizes, and high mesoscopic heterogeneity. It can be described as that under low-stress environment, the micro-fracture initiates from defects with high density and larger scale formed by thermal damage. Non-uniform deformation between mineral particles creates stress concentration, leading to significant stress differences inside the rock. As the microcracks gradually interact and propagate, they gradually expand and penetrate, accompanied by high-frequency and exponential AE activities. On the other hand, in granodiorite, the mechanism of crack evolution can be described as that the small grain size and compactness of mineral particles hinder significant interaction and mutual promotion during crack propagation, resulting in the fluctuation of AE activity. Under thermal expansion, the cohesion increases, indicating a stable internal structure. In addition, the density and scale of pre-existing defects are relatively small, thus the AE activities initiate from higher-stress environments accompanied by low-frequency and oscillation.

The crack propagation mode is controlled by microtextural properties, such as grain sizes and mineral distribution, while the rock crack initiation stress is influenced by the strength of the rock-forming minerals (Eberhardt et al., 1998, 1999). Biotite has the lowest crack initiation stress among all minerals, followed by plagioclase and potassium feldspar. Quartz forms cracks near the damage stress point of granite, and forms predominantly transgranular cracks after reaching the damage stress point (Ghasemi et al., 2020). Meanwhile, the crack around biotite tends to absorb stress, either terminating or deviating from the crack propagation, unless it fractures due to the inability to withstand deformation (Rawling et al., 2002; Mahabadi et al., 2012; Ündül et al., 2013). It can be seen that biotite mainly controls the crack initiation of granodiorite under low-stress environment. Moreover, stress-induced fractures may also occur in other minerals with pre-existing thermal cracks. As the temperature increases, the elastic modulus and toughness of biotite increase, enhancing stress resistance of mineral particles. This implies that the number of intragranular and grain boundary cracks formed by biotite will decrease during the early loading stage. This explains why the secondary crack propagation stage of granodiorite is gradually shortened, and the crack initiation stress point is delayed. Furthermore, as the storage capacity for strain energy increases, the proportion of cracks with large-scale increases at the later loading stage, leading to an increase in the seismic activity for granodiorite. The thermal expansion coefficient of quartz is the highest among the above minerals (Huotari and Kukkonen, 2004), and a large number of intergranular cracks are present in fresh samples (Ghasemi et al., 2020). After increasing the treatment temperature and cooling impact, pre-existing thermal cracks increase due to the gradual growth of intragranular cracking and the elastic mismatch between quartz and other minerals. This leads to the premature release of strain energy under lower stress resulting in gradual advancement of crack propagation stage of granite, and an increase of small-scale microcracks. It explains the increase in the  $b$  value with rising temperature.

#### 4.3. Application

In China, it is estimated that there are recoverable reserves that can meet 5200 times the current total energy consumption within the depth range of 3–10 km. This highlights the enormous potential of dry hot rock resource as alternative energy, which can be used for heating, power generation, and production and living activities after scientific development and utilization. Different dry hot rocks have different physical and mechanical properties as well as damage evolution laws. Therefore, understanding these differences is important for disaster prevention and reduction in the exploration of dry hot rock resources.

The dry hot rock drilling in Gonghe Basin, Qinghai Province, China, serves as an excellent example to validate our results. The hole's final depth is 3705 m, and the rock temperature at the bottom of the hole is 236 °C, and it increases by 8.8 °C every 100 m below 3366 m. Referring to Le Maitre et al. (2005), the rock is a high-quality hot dry rock. The dry hot rock core exhibits extensive transverse fractures, hindering its full extraction. This is closely related to the changes of rock physical and mechanical properties under high temperature and the development of fractures under high stress. Therefore, considering and rationally utilizing the mechanical behavior changes and thermal structural damage characteristics of rocks can improve the selection of drilling plans, processing parameters, drilling fluid, and circulation process, reducing the cost. We take drilling parameter selection as an example. When drilling the granite layers, the bit pressure should decrease slowly with increasing drilling depth and temperature,

but the bit speed can be maintained to suppress the deterioration of the mechanical properties under high temperature. On the other hand, the bit pressure and speed can remain stable for granodiorite layers to ensure drilling efficiency.

## 5. Conclusions

This study conducted a comparison of the temperature dependence of granite and granodiorite under heating and water-cooling by a series of mechanical and AE tests. The two rocks have similar mineralogy and microstructure. We also investigate the mineralogical and structural disparities to shed light on the thermal damage mechanisms of granite and granodiorite. Following are some main conclusions:

- (1) Granodiorite exhibits greater stiffness, strength, and brittleness than granite. The compressive and shear properties of granite and granodiorite have different deterioration trends and transformation thresholds. The physical and mechanical properties of granodiorite alternate between strengthening and weakening under 500 °C. However, the strength of granite gradually decreases with increasing temperature.
- (2) In granite, cracks initiate at lower stress, and coarser grain size and poor meso-heterogeneity promote crack propagation. This leads to a gradual acceleration of nucleation and energy release, resulting in high-frequency, exponential-type AE activity. At the temperature ranges from 100 °C to 500 °C, the crack growth stage extends, accompanied by an increase in the  $b$  value. This can be attributed to a gradual reduction in the secondary cracking threshold and a relatively increased proportion of small-scale micro-fractures.
- (3) In granodiorite, stress concentrations and thermally induced defects are less prominent, leading to localized, small-scale cracking as the main failure mechanism. Consequently, microcracks intermittently nucleate and release energy for multiple times, generating low-frequency, oscillatory-type AE activity. Granodiorite undergoes a transformation in AE temporal evolution characteristics from multi-peak to single-peak, with a shorter secondary crack growth stage. Furthermore, the overall  $b$  value in granodiorite is smaller and tends to decrease with temperature.
- (4) Heating and cooling treatment changes the micro-mechanical properties of minerals, while mesoscopic heterogeneity influences the size and density of thermally induced cracks. Significant distinctions between granite and granodiorite involve enhanced biotite properties, fewer primary defects, finer grain size, and more uniform mineral distribution in granodiorite. The interaction between thermal hardening and thermal cracking effects determines the temperature-dependent mechanical properties and damage evolution.

## Declaration of competing interest

The authors declare that they have no known competing financial interests or personal relationships that could have appeared to influence the work reported in this paper.

## Acknowledgments

The authors would like to acknowledge the financial support from the National Natural Science Foundation of China (Grant No. 52104112), the Research Foundation of the Department of Natural Resources of Hunan Province, China (Grant No. 20230101DZ), and



the Natural Science Foundation of Hunan Province, China (Grant No. 2023JJ20062).

## References

- Bai, M., Reinicke, K.M., Teodoru, C., Fichter, C., 2012. Investigation on water–rock interaction under geothermal hot dry rock conditions with a novel testing method. *J. Pet. Sci. Eng.* 90, 26–30.
- Bao, T., Burghardt, J., 2022. A Bayesian approach for in-situ stress prediction and uncertainty quantification for subsurface engineering. *Rock Mech. Rock Eng.* 55, 4531–4548.
- Brantut, N., 2018. Time-resolved tomography using acoustic emissions in the laboratory, and application to sandstone compaction. *Geophys. J. Int.* 213, 2177–2192.
- Chen, G., Li, T., Zhang, G., Yin, H., Zhang, H., 2014. Temperature effect of rock burst for hard rock in deep-buried tunnel. *Nat. Hazards* 72, 915–926.
- Chen, Y.L., Wang, S.R., Ni, J., Azzam, R., Fernández-steeger, T.M., 2017. An experimental study of the mechanical properties of granite after high temperature exposure based on mineral characteristics. *Eng. Geol.* 220, 234–242.
- Chen, G., Wang, J., Li, J., Li, T., Zhang, H., 2018. Influence of temperature on crack initiation and propagation in granite. *Int. J. GeoMech.* 18, 04018094.
- Chmel, A., Shcherbakov, I., 2014. Temperature dependence of acoustic emission from impact fractured granites. *Tectonophysics* 632, 218–223.
- Dong, L., Zou, W., Li, X., Shu, W., Wang, Z., 2019. Collaborative localization method using analytical and iterative solutions for microseismic/acoustic emission sources in the rockmass structure for underground mining. *Eng. Fract. Mech.* 210, 95–112.
- Dong, L., Hu, Q., Tong, X., Liu, Y., 2020. Velocity-free MS/AE source location method for three-dimensional hole-containing structures. *Engineering* 6, 827–834.
- Dong, L., Tong, X., Hu, Q., Tao, Q., 2021a. Empty region identification method and experimental verification for the two-dimensional complex structure. *Int. J. Rock Mech. Min. Sci.* 147, 104885.
- Dong, L., Chen, Y., Sun, D., Zhang, Y., 2021b. Implications for rock instability precursors and principal stress direction from rock acoustic experiments. *Int. J. Min. Sci. Technol.* 31, 789–798.
- Dong, L., Chen, Y., Sun, D., Zhang, Y., Deng, S., 2022a. Implications for identification of principal stress directions from acoustic emission characteristics of granite under biaxial compression experiments. *J. Rock Mech. Geotech. Eng.* 15 (4), 852–863.
- Dong, L., Zhang, Y., Sun, D., Chen, Y., Tang, Z., 2022b. Stage characteristics of acoustic emission and identification of unstable crack state for granite fractures. *Chin. J. Rock Mech. Eng.* 41, 120–131 (in Chinese).
- Dong, L., Bi, S., Zhang, Y., Hu, Q., Zhu, H., 2023a. Arrival time detection with multiscale wavelet analysis and source location of acoustic emission in rock. *IEEE Sensor. J.* 23, 16313–16323.
- Dong, L., Yang, L., Chen, Y., 2023b. Acoustic emission location accuracy and spatial evolution characteristics of granite fracture in complex stress conditions. *Rock Mech. Rock Eng.* 56, 1113–1130.
- Eberhardt, E., Stead, D., Stimpson, B., Read, R.S., 1998. Identifying crack initiation and propagation thresholds in brittle rock. *Can. Geotech. J.* 35, 222–233.
- Eberhardt, E., Stimpson, B., Stead, D., 1999. Effects of grain size on the initiation and propagation thresholds of stress-induced brittle fractures. *Rock Mech. Rock Eng.* 32, 81–99.
- Feng, Y., Harrison, J.P., Bozorgzadeh, N., 2021. A Bayesian approach for uncertainty quantification in overcoring stress estimation. *Rock Mech. Rock Eng.* 54, 627–645.
- Ge, Z., Sun, Q., 2018. Acoustic emission (AE) characteristics of granite after heating and cooling cycles. *Eng. Fract. Mech.* 200, 418–429.
- Ghasemi, S., Khammehchiyan, M., Taheri, A., Reza, M., Ahmad, N., 2020. Crack evolution in damage stress thresholds in different minerals of granite rock. *Rock Mech. Rock Eng.* 53, 1163–1178.
- Güneş Yılmaz, N., Mete Goktan, R., Kibici, Y., 2011. Relations between some quantitative petrographic characteristics and mechanical strength properties of granitic building stones. *Int. J. Rock Mech. Min. Sci.* 48, 506–513.
- Guo, Q., Su, H., Liu, J., Yin, Q., Jing, H., Yu, L., 2020. An experimental study on the fracture behaviors of marble specimens subjected to high temperature treatment. *Eng. Fract. Mech.* 225, 106862.
- He, A., Wang, Z., Shi, H., 2018. Strength characteristics and mineral component variations of heat-treated granite. *J. Hefei Univ. Technol. (Nat. Sci.)* 41, 501–506.
- Huang, Y.H., Yang, S.Q., Tian, W.L., Zhao, J., Ma, D., Zhang, C.S., 2017. Physical and mechanical behavior of granite containing pre-existing holes after high temperature treatment. *Arch. Civ. Mech. Eng.* 17, 912–925.
- Hudson, R., Ulusay, J.A., 2007. *The ISRM Suggested Methods for Rock Characterization, Testing and Monitoring: 2007–2014*. Springer.
- Huotari, T., Kukkonen, I., 2004. Thermal expansion properties of rocks: literature survey and estimation of thermal expansion coefficient for Olkiluoto mica gneiss. *Posiva Oy, Olkiluoto, Work. Rep.* 4, 62.
- Kang, F., Li, Y., Tang, C., 2021. Grain size heterogeneity controls strengthening to weakening of granite over high-temperature treatment. *Int. J. Rock Mech. Min. Sci.* 145, 104848.
- Kimizuka, H., Kaburaki, H., Kogure, Y., 2003. Molecular-dynamics study of the high-temperature elasticity of quartz above the  $\alpha$ - $\beta$  phase transition. *Phys. Rev. B* 67, 24105.
- Kong, R., Tuncay, E., Ulusay, R., Zhang, X., Feng, X.T., 2021. An experimental investigation on stress-induced cracking mechanisms of a volcanic rock. *Eng. Geol.* 280, 105934.
- Kumari, W.G.P., Ranjith, P.G., Perera, M.S.A., Chen, B.K., Abdulgatov, I.M., 2017. Temperature-dependent mechanical behavior of Australian Strathbogie granite with different cooling treatments. *Eng. Geol.* 229, 31–44.
- Kwiatek, G., Charalampidou, E.M., Dresen, G., Stanchits, S., 2014. An improved method for seismic moment tensor inversion of acoustic emissions through assessment of sensor coupling and sensitivity to incidence angle. *Int. J. Rock Mech. Min. Sci.* 65, 153–161.
- Le Maitre, R.W., Streckeisen, A., Zanettin, B., Le Bas, M.J., Bonin, B., Bateman, P., 2005. *Igneous Rocks: A Classification and Glossary of Terms: Recommendations of the International Union of Geological Sciences Subcommission on the Systematics of Igneous Rocks*. Cambridge University Press.
- Lei, X.L., Kusunose, K., Nishizawa, O., Cho, A., Satoh, T., 2000. On the spatio-temporal distribution of acoustic emissions in two granitic rocks under triaxial compression: the role of pre-existing cracks. *Geophys. Res. Lett.* 27, 1997–2000.
- Lei, X., 2003. How do asperities fracture? An experimental study of unbroken asperities. *Earth Planet. Sci. Lett.* 213, 347–359.
- Lei, X.L., 2017. Laboratory acoustic emission study review. In: *Rock Mechanics and Engineering*, ume 2, pp. 127–164. CRC Press.
- Li, L., Lee, P.K.K., Tsui, Y., Tham, L.G., Tang, C.A., 2003. Failure process of granite. *Int. J. GeoMech.* 3, 84–98.
- Li, N., Zhang, S., Ma, X., Zou, Y., Li, S., Zhang, Z., 2020. Thermal effect on the evolution of hydraulic fracture conductivity: an experimental study of enhanced geothermal system. *J. Pet. Sci. Eng.* 187, 106814.
- Li, H.R., Wang, Z.H., Meng, S.R., Zhao, W.G., Chen, F., 2021. Acoustic emission activity and damage evolution characteristics of marble under triaxial stress at high temperatures. *Yantu Lixue/Rock Soil Mech.* 42, 2672–2682.
- Lindqvist, J.E., Åkesson, U., Malaga, K., 2007. Microstructure and functional properties of rock materials. *Mater. Char.* 58, 1183–1188.
- Liu, S., Li, X., Wang, D., Wu, M., Yin, G., Li, M., 2020b. Mechanical and acoustic emission characteristics of coal at temperature impact. *Nat. Resour. Res.* 29, 1755–1772.
- Liu, S., Xu, J., 2014. Mechanical properties of Qinling biotite granite after high temperature treatment. *Int. J. Rock Mech. Min. Sci.* 71, 188–193.
- Liu, X., Liu, Z., Li, X., Gong, F., Du, K., 2020a. Experimental study on the effect of strain rate on rock acoustic emission characteristics. *Int. J. Rock Mech. Min. Sci.* 133, 104420.
- Ma, T., Zhu, G., Peng, N., Qiu, Y., Liu, Y., Zou, J., 2021. Physical-mechanical properties and thermally-induced damage of granite after high-temperature pretreatment. *Arabian J. Geosci.* 14, 1449.
- Ma, X., Wang, G., Hu, D., Liu, Y., Zhou, H., Liu, F., 2020. Mechanical properties of granite under real-time high temperature and three-dimensional stress. *Int. J. Rock Mech. Min. Sci.* 136, 104521.
- Mahabadi, O.K., Randall, N.X., Zong, Z., Grasselli, G., 2012. A novel approach for micro-scale characterization and modeling of geomaterials incorporating actual material heterogeneity. *Geophys. Res. Lett.* 39.
- Mo, C., Zhao, J., Zhang, D., 2022. Real-time measurement of mechanical behavior of granite during heating-cooling cycle: a mineralogical perspective. *Rock Mech. Rock Eng.* 55, 4403–4422.
- Moura, A., Lei, X., Nishisawa, O., 2005. Prediction scheme for the catastrophic failure of highly loaded brittle materials or rocks. *J. Mech. Phys. Solid.* 53, 2435–2455.
- Moura, A., Lei, X., Nishisawa, O., 2006. Self-similarity in rock cracking and related complex critical exponents. *J. Mech. Phys. Solid.* 54, 2544–2553.
- Ohno, I., 1995. Temperature variation of elastic properties of  $\alpha$ -quartz up to the  $\alpha$ - $\beta$  transition. *J. Phys. Earth* 43, 157–169.
- Ohno, I., Harada, K., Yoshitomi, C., 2006. Temperature variation of elastic constants of quartz across the  $\alpha$ - $\beta$  transition. *Phys. Chem. Miner.* 33, 1–9.
- Peng, J., Wong, L.N.Y., Teh, C.I., 2021. Influence of grain size on strength of polycrystalline rock: new insights from DEM grain-based modeling. *J. Rock Mech. Geotech. Eng.* 13, 755–766.
- Prodaivoda, G.T., Maslov, B.P., Prodaivoda, T.G., 2004. Estimation of thermoelastic properties of rock-forming minerals. *Russ. Geol. Geophys.* 45, 389–404.
- Rawling, G.C., Baud, P., Wong, T., 2002. Dilatancy, brittle strength, and anisotropy of foliated rocks: experimental deformation and micromechanical modeling. *J. Geophys. Res. Solid Earth* 107, ETG-8.
- Su, G., Chen, Z., Ju, J.W., Jiang, J., 2017. Influence of temperature on the strainburst characteristics of granite under true triaxial loading conditions. *Eng. Geol.* 222, 38–52.
- Talukdar, M., Guha Roy, D., Singh, T.N., 2018. Correlating mode-I fracture toughness and mechanical properties of heat-treated crystalline rocks. *J. Rock Mech. Geotech. Eng.* 10, 91–101.
- Ündül, Ö., Amann, F., Aysal, N., Plötze, M., 2013. Micro-textural controlled variations of the geomechanical properties of andesites. In: *ISRM International Symposium-EUROCK 2013*. OnePetro.
- Ündül, Ö., Amann, F., Plötze, M.L., 2015. Micro-textural effects on crack initiation and crack propagation of andesitic rocks. *Eng. Geol.* 193, 267–275.
- Wang, Z., He, A., Shi, G., Mei, G., 2018. Temperature effect on AE energy characteristics and damage mechanical behaviors of granite. *Int. J. GeoMech.* 18, 04017163.
- Wei, G., Meng, J., Du, X., Yang, Y., 2015. Performance analysis on a hot dry rock geothermal resource power generation system based on Kalina cycle. *Energy Proc.* 75, 937–945.

- Wu, X., Huang, Z., Song, H., Zhang, S., Cheng, Z., Li, R., Wen, H., Huang, P., Dai, X., 2019. Variations of physical and mechanical properties of heated granite after rapid cooling with liquid nitrogen. *Rock Mech. Rock Eng.* 52, 2123–2139.
- Wu, Y., Li, X.Z., Huang, Z., Xue, S., 2021. Effect of temperature on physical, mechanical and acoustic emission properties of Beishan granite, Gansu Province, China. *Nat. Hazards* 107, 1577–1592.
- Xu, X.L., Zhang, Z.-Z., 2018. Acoustic emission and damage characteristics of granite subjected to high temperature, 2018 *Adv. Mater. Sci. Eng.* 1–12.
- Xiao, W., Zhang, D., Yang, H., Yu, B., Li, S., 2022. Evaluation and analysis of sandstone brittleness under the influence of temperature. *Geomech. Geophys. Geo-Energy Geo-Resources* 8, 1–19.
- Xing, Y., Zhang, G., Luo, T., Jiang, Y., Ning, S., 2019. Hydraulic fracturing in high-temperature granite characterized by acoustic emission. *J. Pet. Sci. Eng.* 178, 475–484.
- Yang, S.Q., Huang, Y.H., Tian, W.L., Yin, P.F., Jing, H.W., 2019. Effect of high temperature on deformation failure behavior of granite specimen containing a single fissure under uniaxial compression. *Rock Mech. Rock Eng.* 52, 2087–2107.
- Yang, Y., Wang, Z.P., Tian, Z.Z., Xia, Q.K., Li, G.W., 2016. High-temperature phase transition and local structure of a hydrous anorthoclase. *Phys. Chem. Miner.* 43, 111–118.
- Yang, Z., Yin, T., Zhuang, D., Wu, Y., Yin, J., Chen, Y., 2022. Effect of temperature on mixed mode I/III fracture behavior of diorite: an experimental investigation. *Theor. Appl. Fract. Mech.* 122, 103571.
- Yin, T., Yang, Z., Wu, Y., Tan, X., Li, M., 2022. Experimental investigation on the effect of open fire on the tensile properties and damage evolution behavior of granite. *Int. J. Damage Mech.* 31, 1139–1164.
- Zhang, F., Hu, W., Guo, H., Hu, D., Sheng, Q., Shao, J., 2018b. Nanoindentation tests on granite after heat treatment. *Rock Soil Mech.* 39, 235–243.
- Zhang, F., Zhao, J., Hu, D., Skoczylas, F., Shao, J., 2018a. Laboratory investigation on physical and mechanical properties of granite after heating and water-cooling treatment. *Rock Mech. Rock Eng.* 51, 677–694.
- Zhang, W., Sun, Q., 2018. Identification of primary mineral elements and macroscopic parameters in thermal damage process of limestone with canonical correlation analysis. *Rock Mech. Rock Eng.* 51, 1287–1292.
- Zhao, X.G., Cai, M., Wang, J., Li, P.F., Ma, L.K., 2015a. Objective determination of crack initiation stress of brittle rocks under compression using AE measurement. *Rock Mech. Rock Eng.* 48, 2473–2484.
- Zhao, Y.S., Feng, Z.J., Xi, B.P., Yang, D., Liang, W.G., Wan, Z.J., 2017a. Limit of crustal drilling depth. *J. Rock Mech. Geotech. Eng.* 9, 989–992.
- Zhao, Y.S., Wan, Z.J., Feng, Z.J., Xu, Z.H., Liang, W.G., 2017b. Evolution of mechanical properties of granite at high temperature and high pressure. *Geomech. Geophys. Geo-Energy Geo-Resources* 3, 199–210.
- Zhao, Y.S., Feng, Z.J., Xi, B.P., Wan, Z.J., Yang, D., Liang, W.G., 2015b. Deformation and instability failure of borehole at high temperature and high pressure in hot dry rock exploitation. *Renew. Energy* 77, 159–165.
- Zhao, Z., Liu, Z., Pu, H., Li, X., 2018. Effect of thermal treatment on Brazilian tensile strength of granites with different grain size distributions. *Rock Mech. Rock Eng.* 51, 1293–1303.



**Lichang Wang** received his PhD from the School of Geosciences and Info-physics, Central South University, Changsha, China. Currently, he is a lecturer at the same university. His research interests include deep drilling rock mechanics, crystalline mineral mechanics, and methods for locating and identifying seismic sources. Dr. Wang's work has been supported by the National Natural Science Foundation of China, the National Key Research and Development Program of China, and the Hunan Provincial Natural Science Foundation for Excellent Young Scholars. He has authored over 40 papers published in related journals and holds more than 10 patents. He is a member of the expert panel of International Society for Trenchless Technology (ISTT) and China Society of Geology-Trenchless Technology Committee (CSTT).